Oxygen Vacancy-Mediated High-Entropy Oxide Electrocatalysts for Efficient Oxygen Evolution Reaction

Ruonan Liu, Yaotian Yan, Liang Dun, Taili Yang, Qin Bin, Peijia Wang, Wei Cai, Shude Liu, Xiaohang Zheng

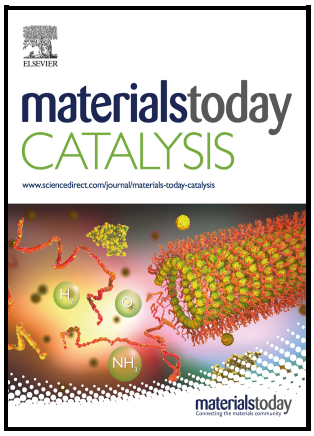

PII: S2949-754X(24)00048-6

DOI: https://doi.org/10.1016/j.mtcata.2024.100086

Reference: MTCATA100086

To appear in: *Materials Today Catalysis*

Received date: 20 October 2024
Revised date: 3 December 2024
Accepted date: 23 December 2024

Please cite this article as: Ruonan Liu, Yaotian Yan, Liang Dun, Taili Yang, Qin Bin, Peijia Wang, Wei Cai, Shude Liu and Xiaohang Zheng, Oxygen Vacancy-Mediated High-Entropy Oxide Electrocatalysts for Efficient Oxygen Evolution Reaction, *Materials Today Catalysis,* (2024) doi:https://doi.org/10.1016/j.mtcata.2024.100086

Oxygen Vacancy-Mediated High-Entropy Oxide Electrocatalysts for Efficient Oxygen Evolution Reaction

Ruonan Liu[1], Yaotian Yan[1,*], Liang Dun[1], Taili Yang[1], Qin Bin[2], Peijia Wang[1], Wei Cai [1], Shude Liu[3,4,*] and Xiaohang Zheng[1,*]

[1] School of Materials Science and Engineering, Harbin Institute of Technology, Harbin, China

[2] Key Laboratory of Magnetic Molecules and Magnetic Information Materials of Ministry of Education & School of Chemistry and Materials Science, Shanxi Normal University, Taiyuan, 030032, China

[3] Engineering Research Center of Technical Textile, Ministry of Education, College of Textiles, Donghua University, Shanghai 201620, P. R. China

[4] Department of Materials Process Engineering, Graduate School of Engineering, Nagoya University, Nagoya 464-8603, Japan

[*]Correspondence author. Email: ytyanhit@hit.edu.cn (Y. Yan); sdliu@dhu.edu.cn (S. Liu); zhengxiaohang@hit.edu.cn (X. Zheng).

Keywords: high-entropy oxide, oxygen evolution reactions, non-equilibrium thermal shock, electrocatalysis

ABSTRACT

Transition metal oxides hold great potential for water splitting due to their tunable electronic structures and abundant availability. However, their inherently poor electrical conductivity and limited catalytic activity hinder their practical implementation. Herein, high-entropy oxide (FeCoNiCrCuO) electrocatalysts featuring grain-like structure and oxygen vacancies-enriched surface were synthesized through an ultra-fast non-equilibrium high-temperature shock. The introduction of oxygen vacancies modulates the electronic structure and increases the carrier concentration, accelerating the rate-determining step of the oxygen evolution reactions and reducing the overpotential of oxygen evolution reactions. Consequently, the synthesized FeCoNiCrCuO electrocatalyst delivers a low overpotential of 256 mV at a current density of 10 $mA \cdot cm^{-2}$ and a Tafel slope of 48.2 $mV \cdot dec^{-1}$ in 1 M KOH, which is superior to samples lacking oxygen vacancies after annealing. This study presents an alternative approach to enhancing OER activity by employing a high-entropy oxide engineering strategy.

INTRODUCTION

Water electrolysis, a dominant method for hydrogen production, is hindered by the sluggish kinetics of the oxygen evolution reaction, leading to significant overpotential[1, 2]. To address this limitation, catalysts are essential. Currently, catalysts are categorized into two groups: noble metal-based (RuO_2 and IrO_2) and non-noble metal-based. While noble metal catalysts exhibit exceptional OER performance, their scarcity and high costs limit industrial adoption. Therefore, the development of high-performance, stable,

and noble metal-free catalysts is crucial for the practical integration of hydrogen energy. OER catalysts primarily encompass transition metal oxides, phosphides, carbides, nitrides, sulfides, alloys, and a range of non-metallic catalysts[3-5]. Among them, transition metal oxides have garnered considerable attention due to their natural abundance, low cost, structural tunability, and exceptional stability, making them a promising candidate for the development of a low-cost, highly active, and durable electrocatalyst[6, 7]. Nevertheless, the inherently poor electrical conductivity and scarcity of active sites in most oxides are significant obstacles to their development as efficient electrocatalysts.

Transition metal-based high-entropy oxides are considered promising electrocatalysts due to their huge reserves, low prices, and the four primary effects (high entropy effect, sluggish diffusion effect, severe lattice distortion, and the cocktail effect)[8-10]. The high-entropy effect makes the oxides more stable, while the synergy of multiple elements enhances the intrinsic activity of the catalyst, providing more diverse active sites, which is beneficial for oxygen evolution reaction. However, poor conductivity still the ability of oxides to serve as highly efficient catalysts for oxygen evolution reactions. Typically, oxides possess a wide bandgap, and strong bonds between oxygen atoms and metals constrain electrons to atomic orbitals, making transitions from the valence band to the conduction band challenging, thereby limiting their conductivity. However, the presence of oxygen vacancies reduces electron localization in the vicinity and acts as electron donors, introducing additional electrons or increasing defect states, which elevate the carrier concentration of the oxide, improving conductivity, and thus

enhancing the performance of the oxygen evolution reaction[11-14]. Recently, Yao et al. [15] reported a novel approach for the synthesis of high-entropy alloys. By the Joule heating effect, the temperature of the materials is raised from room temperature to high temperature (up to approximately 2000 K) in an extremely short period. Subsequently, the materials rapidly cool to room temperature, a consequence of the limited thermal diffusion length. The non-equilibrium thermal shock not only enables the rapid synthesis of high entropy alloys, but the non-equilibrium process of rapid cycling of temperature brings rich lattice defects[16-20]. Considering that oxygen atoms are more prone to detachment at high temperatures, forming oxygen vacancies, the utilization of non-equilibrium thermal shock for the fabrication of high-entropy oxides is anticipated to yield favorable outcomes.

Herein, we report an oxygen-deficient FeCoNiCrCu high-entropy oxide (FeCoNiCrCuO) electrocatalyst synthesized by a non-equilibrium thermal shock to enhance OER. The properties of FeCoNiCrCuO and FeCoNiCrCuO prepared by a general annealing process (FeCoNiCrCuO-A1 and FeCoNiCrCuO-A2) were compared. XPS shows that the content of vacancy oxygen in FeCoNiCrCuO-A1 and FeCoNiCrCuO-A2 is lower than that in FeCoNiCrCuO. DFT calculations indicate that the presence of oxygen vacancies modulates the d-band center of the FeCoNiCrCuO and accelerates the rate determining step of the oxygen evolution reactions. And The results show that the FeCoNiCrCuO electrocatalyst exhibits excellent OER activity with a small overpotential of 256 mV at 10 $mA \cdot cm^{-2}$ and a Tafel slope of 48.2 $mV \cdot dec^{-1}$. In contrast, the FeCoNiCrCuO-A1 and FeCoNiCrCuO-A2 electrocatalyst

demonstrate a deteriorated OER activity, with an overpotential of 280 mV and 437 mV. The superior properties of the FeCoNiCrCuO electrocatalyst confirm that engineering high-entropy oxides can effectively enhance OER electrocatalytic performance.

RESULTS AND DISCUSSION

The catalyst was synthesized using the thermal shock method. During the process, the changes in current and temperature are shown in Figure S1. X-ray diffraction (XRD) is employed for the characterization of the phase. As shown in Figure 1a, the graphs depict the curves of FeCoNiCrCuO, FeCoNiCrCuO-A1 and FeCoNiCrCuO-A2, and the standard PDF cards for $CoCr_2O_4$(78-0711), arranged in a top-to-bottom sequence. The peaks located near 25 ° and 43 ° belong to carbon substrates. The diffraction peaks of two samples near 30.06 °, 35.45 °, 37.28 °, 43.47 °, 53.88 °, 57.16 °, and 62.72 ° correspond well to the standard structure of $CoCr_2O_4$ phase[21-23]. It indicates that the prepared catalyst is a high-entropy oxide with a single-phase spinel structure. Raman spectroscopy showed no significant changes in the three samples (Figure 1b). The technique of scanning electron microscopy (SEM) is employed for the examination and analysis of the microstructure of a sample's surface. To confirm the surface oxygen vacancy of catalyst, the electron paramagnetic resonance (EPR) spectroscopy was conducted. As shown in Figure 1c, the characteristic signals at g = 2.003 arisen from unpaired electrons of oxygen vacancy are conspicuous. The signal intensity from the FeCoNiCrCuO sample is significantly larger than that from the FeCoNiCrCuO-A1 or FeCoNiCrCuO-A2 sample, indicating more oxygen vacancy in FeCoNiCrCuO. Figure

S2 show the surface micromorphology of FeCoNiCrCuO, FeCoNiCrCuO-A1 and FeCoNiCrCuO-A2, respectively, which are irregular lumps adhering to carbon fibers and exhibit variable dimensions spanning from tens to hundreds of nanometers. Furthermore, it is observed that their structural form remains unaltered before and after undergoing heat treatment, indicating that the thermal process does not affect their external morphology. As shown in Figures 1d and 1e, TEM images of FeCoNiCrCuO show a particle structure with a size of from ~20 to ~300 nm. HRTEM image (Figure 1f) reveals a lattice spacing of approximately 0.250 nm and 0.290 nm, corresponding to the (311) and (220) crystal planes of the $CoCr_2O_4$ phase. The defects can be observed in Figure 1f (marked by the yellow circle), which proves that non-equilibrium thermal shock can induce lattice distortion. As shown in Figure S3, it is the HRTEM processed by Fast Fourier Transform (FFT) and Inverse FFT, which provides a more intuitive demonstration of the state of the lattice fringes and enables the clear observation of dislocation and lattice distortion. As shown in Figure 1g, it is the elemental energy spectrum mapping on FeCoNiCrCuO, purple is Co, green is Cr, blue-green is Cu, blue is Fe, brown is Ni and red is O. The elemental energy spectrum mapping demonstrates the even distribution of Fe, Cr, Co, Cu, Ni and O within the nanoparticles, which proves the elemental distribution uniformity.

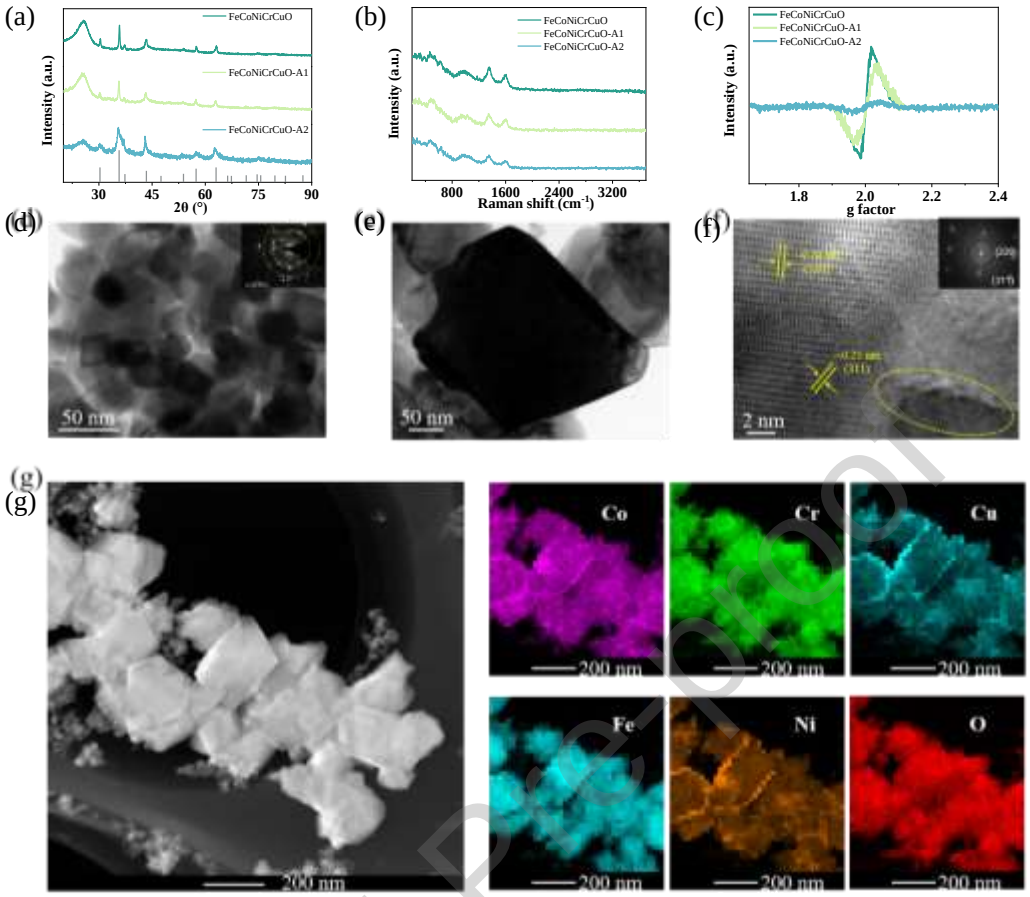

Figure 1 (a) XRD pattern of FeCoNiCrCuO, FeCoNiCrCuO-A1 and FeCoNiCrCuO-A2. (b) Raman of FeCoNiCrCuO, FeCoNiCrCuO-A1 and FeCoNiCrCuO-A2. (c) EPR of FeCoNiCrCuO, FeCoNiCrCuO-A1 and FeCoNiCrCuO-A2. (d) and (e) TEM images on FeCoNiCrCuO. (f) High-resolution transmission electron microscope (HRTEM) on FeCoNiCrCuO. (g) Elemental energy spectrum mapping on FeCoNiCrCuO.

To further investigate the electronic structure and the alteration of the synthesized FeCoNiCrCuO, FeCoNiCrCuO-A1 and FeCoNiCrCuO-A2, the elemental composition and surface chemical valence states are tested using XPS. As shown in Figure S4, the characteristic peaks in the full spectrum of the three samples correspond to C 1s, O 1s, Cr 2p, Fe 2p, Co 2p, Ni 2p, and Cu 2p, respectively. This proves that the catalyst contains seven elements: Co, C, Cr, O, Fe, Ni, and Cu. The high-resolution O 1s XPS

spectrum reveals three peaks (Figures 2a, 2b and 2c): ~529.9 eV ascribed to the lattice oxygen, ~532.6 eV attributed to surface-adsorbed hydroxyl species, and ~531.2 eV caused by the chemisorption of oxygen vacancies, which is a typical feature of oxygen vacancies[24-26]. The peak area of FeCoNiCrCuO at 531.2 eV is 46.9%, which is the larger value compared with FeCoNiCrCuO-A1 (37.8%) and FeCoNiCrCuO-A2 (18.6%), which is consistent with EPR and the performance test results. The presence of defects, particularly oxygen vacancies, enhances the number of active sites on the catalyst and facilitates charge transfer, consequently influencing its performance. Figures 2d, 2e and 2f display the high-resolution XPS spectra of Co 2p. The XPS spectrum of Co $2p_{3/2}$ was fitted with two peaks at ~780.0 and ~782.0 eV, which are ascribed to the Co^{3+} and Co^{2+} species, respectively. From the XPS results, the Co^{2+}/Co^{3+} ratio for FeCoNiCrCuO is ~1.29, while that for FeCoNiCrCuO-A1 and FeCoNiCrCuO-A2 are only ~0.35 and 0.26, respectively. In some cobalt-based oxides, the generation of oxygen vacancies leads to a redistribution of electrons, causing some Co^{3+} ions to gain electrons and transform into Co^{2+} ions to compensate for the charge imbalance caused by oxygen vacancies[27]. According to report of Wang et al., the Co^{2+}/Co^{3+} ratio for Co_3O_4 which has the most oxygen vacancies is ~1.0, while those for lower are only ~0.60[28]. In the other work, the formation of oxygen vacancies in La-doped CoO_x can be ascribed to the La-induced partial reduction from Co^{3+} to Co^{2+}[29]. Therefore, a higher Co^{2+}/Co^{3+} indicates more oxygen vacancies, which further verifies the presence of higher oxygen vacancy density in FeCoNiCrCuO[30]. Figure S5 showes XPS spectra of Fe 2p, based on the location of the satellite, it can be determined that the peak at near 711.3 eV is ascribed to the Fe^{3+}. Figure S6 showes XPS spectra of Ni 2p, the peak at near 855.5 eV is ascribed to the Ni^{2+}. Figure S7 showes XPS spectra of Cr 2p, the peak at near 576.5 eV is ascribed to the Cr^{3+}. Figure S8 showes XPS spectra of Cu 2p, based on the location of the satellite, the peak at near 933 eV is ascribed to the Cu^{2+}. The comparative sample was oxidized through heat treatment in air to decrease the oxygen vacancies. There was no significant alteration in the valence states of other metal elements, except for the increase in Co^{3+} content.

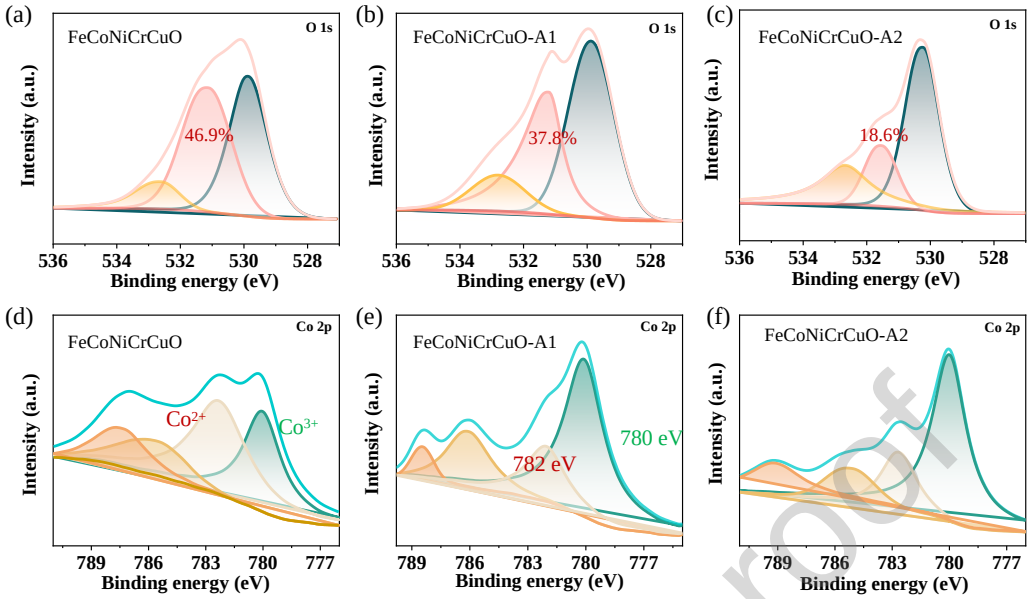

Figure 2 (a) High-resolution XPS spectra of O1s for FeCoNiCrCuO. (b) High-resolution XPS spectra of O 1s for FeCoNiCrCuO-A1. (c) High-resolution XPS spectra of O 1s for FeCoNiCrCuO-A2. (d) High-resolution XPS spectra of Co 2p for FeCoNiCrCuO. (e) High-resolution XPS spectra of Co 2p for FeCoNiCrCuO-A1. (f) High-resolution XPS spectra of Co 2p for FeCoNiCrCuO-A2.

The assessment of the electrocatalytic performance was carried out using a three-electrode system and an electrochemical workplace (Chi 760e), with a 1.0 M KOH as electrolyte and the mercury/mercury oxide electrode as the reference electrode. Cyclic voltammetry (CV) is utilized to initialize the catalyst surface, followed by the probing of OER activity through linear sweep voltammetry (LSV). As shown in Figure 3, the electrochemical performance test results are illustrated. As shown in Figure 3a, it can be intuitively seen that FeCoNiCrCuO performs better than FeCoNiCrCuO-A1 and FeCoNiCrCuO-A2, which is consistent with the previous analysis. The overpotential at 10 $mA \cdot cm^{-2}$ is employed as the principal metric for evaluating the efficacy of HEO catalysts. The overpotential of FeCoNiCrCuO is 256 mV at 10 $mA \cdot cm^{-2}$, while under

identical test conditions, FeCoNiCrCuO-A1 and FeCoNiCrCuO-A2 are 280 mV and 437 mV, respectively. To identify the reaction mechanism, a Tafel plot is constructed by selecting the linear region of the polarization curve and fitting it to the Butler-Volmer equation. Figure 3c shows that the Tafel slopes of FeCoNiCrCuO, FeCoNiCrCuO-A1 and FeCoNiCrCuO-A2 are 48.2, 73.0 $mV \cdot dec^{-1}$ and 177 $mV \cdot dec^{-1}$, respectively. A steeper slope of the catalyst results in a slower rate of charge transfer. Obviously, the Tafel slope of FeCoNiCrCuO is shallower and the reaction kinetics are faster. EIS is another effective method for characterizing interfacial reactions and electrode kinetics. The diameter of the semicircle prior to the curve inflection point signifies the charge transfer resistance (R_{ct}), with smaller resistance indicating faster charge transfer. Through fitting, the R_{ct} of FeCoNiCrCuO is determined to be 1.184 Ω, whereas that of FeCoNiCrCuO-A1 and FeCoNiCrCuO-A2 are found to be 4.031 Ω and 6.610 Ω (Figure 3d). It indicates that the charge transfer rate of FeCoNiCrCuO is faster, which aligns with the increasing tendency of OER activity and demonstrates the influence of oxygen vacancies on charge transfer. Furthermore, the electrochemical surface area (ECSA) of the samples is used to estimate the number of active sites exposed by the electrocatalyst, which can be assessed by calculating the double-layer capacitance (C_{dl}) of the CV curves (Figure S9). Figure 3e shows that FeCoNiCrCuO (47.2 mF cm^{-2}) presents a considerably larger C_{dl} than the FeCoNiCrCuO-A1 (18.5 mF cm^{-2}) and FeCoNiCrCuO-A2 (6.0 mF cm^{-2}), indicating that much more active sites are exposed in the OER test due to the introduction of oxygen vacancies. FeCoNiCrCuO was firstly swept between 0 and 1 V for 4000 cycles with a scan rate of 50 mV s^{-1}, then the polarization curve was

measured. As a result, the overpotential only increases 13 mV at 10 mA cm^{-2} relative to the initial electrocatalytic polarization curve (Figure 3f). As shown in Figure 3g, the overall voltage fluctuation within ~80 hours is negligible, which is due to the entropy stability driven by high entropy. Figure S10 show the XPS, XRD, and SEM of the electrocatalyst after stability test. The high-resolution O 1s reveal a decrease in the proportion of peaks corresponding to oxygen vacancies. And as shown in Co 2p XPS spectra, the ratio of Co^{2+}/Co^{3+} is decreased to 0.86. Additionally, there was no significant change in the morphology and crystal phase. Significantly, as shown in Figure 3h, the performance of the samples in this study is represented by the dark green bar on the far left, while the light green bar on the right depicts the performance of previously published work. It is evident that the orange bar appears to be the shortest, and our catalyst performance is superior to some of previously reported oxide catalysts[31-39], which confirms that FeCoNiCrCuO by the non-equilibrium thermal shock is being recognized as a promising and efficient catalyst for OER in water splitting applications.

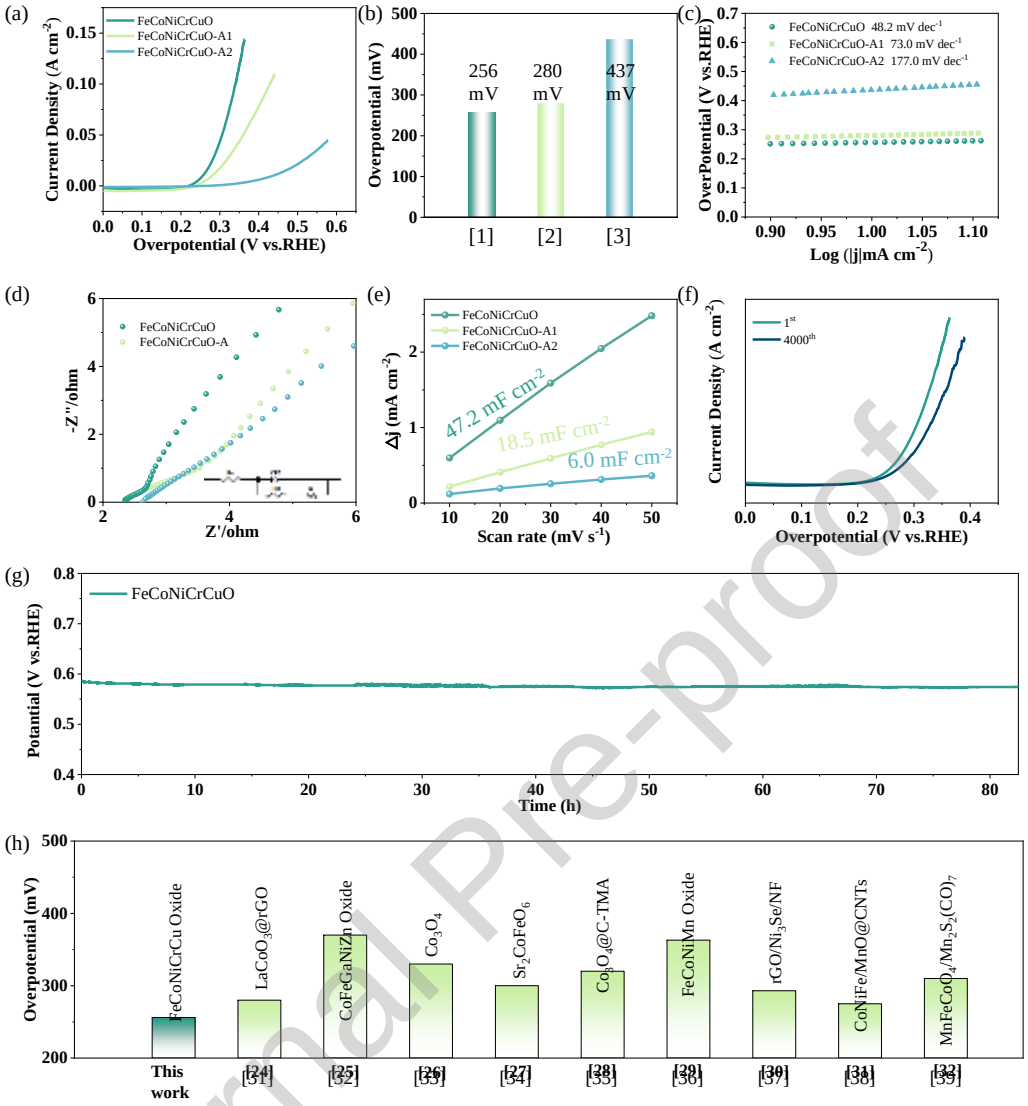

Figure 3 Electrochemical performance analysis. (a) LSV scans for catalysts prepared. (b) Bar chart of overpotential of the catalysts ([1] FeCoNiCrCuO, [2] FeCoNiCrCuO-A1, [3] FeCoNiCrCuO-A2). (c) Tafel slopes for catalysts prepared. (d) Nyquist plots. (e) Plots showing extraction of the double-layer capacitance (Cdl). (f) LSV scans for FeCoNiCrCuO on the first and after 4000 cycles. (g) The long-term stability test lasting for ~80 h. (h) Overpotential of other reports for comparison.

OER involves four sequential reaction steps, each involving the transfer of one electron, with the rate-determining step (RDS) being that with the largest energy barrier, as shown in Figure 4a. The OER four-electron transfer process was calculated using density functional theory to determine its free energy change. Based on XRD results,

$CoCr_2O_4$ (78-0711) was chosen as the parent structure for generating the HEO structure with the optimized lattice parameters (a = b = c = 8.335 Å)[40]. As illustrated in Figure S11, the two computational models are representative of FeCoNiCrCuO and FeCoNiCrCuO-A, respectively, with the yellow circles denoting oxygen vacancy sites. To simulate the disorderliness of high-entropy oxides, the metal atoms in the parent structure are substituted by an equal molar ratio of five types of atoms in a random replacement approach. As shown in Figures 4b and S12, it was found that with the introduction of oxygen vacancy, the d-band center of Fe, Co, Ni, Cr and Cu are decreased. Especially, the d-band center of Co decreased from −1.325 eV to −1.371 eV, and that the declining d-band center will lead to more occupation of the antibonding state between the metal surface and the adsorbate, thus weakening the bonding strength of the oxygen-containing intermediate and reducing the formation energy barrier of the intermediate[41, 42]. As shown in Figures 4d and 4e, theoretical calculations indicate that the Gibbs free energies of the four reactions for the FeCoNiCrCuO (Co site) are calculated to be -1.08, 2.83, 0.92 and 2.25 eV, respectively. The Gibbs free energies of the four reactions for the FeCoNiCrCuO-A (Co site) are calculated to be 9.51, 5.34, -8.05 and -1.88 eV, respectively. The calculation results for the other four active sites, Fe site, Ni site, Cr site, and Cu site, are also shown in Figures 4d and 4e. As shown in Figure 4c, the maximum energy barriers of the Fe, Co, Ni, Cr, and Cu sites were 4.08, 2.83, 3.53, 15.23 and 10.18 eV, respectively, indicating that the Co and Ni site was the main active site of the FeCoNiCrCuO. The energy difference of FeCoNiCrCuO with oxygen vacancies in the rate determination step is lower than that of FeCoNiCrCuO-A.

This observation suggests that the presence of oxygen vacancies can facilitate the OER process.

Based on the analysis of the above results, during the non-equilibrium thermal shock process, five metal elements are blended and react with oxygen to produce granular high-entropy oxides. Numerous oxygen vacancies are introduced by non-equilibrium thermal shock, which increases the number of exposed active sites, reduces the energy difference of the speed determination step, and boosts the electrical conductance of transition metal catalyst systems[43, 44]. Meanwhile, high-entropy oxides have excellent performance in structural, thermodynamic, and kinetic properties due to disordered atom distribution[45]. This study shows a bright prospect of low-cost high entropy oxides in water splitting and will offer significant insights for the development of superior OER catalysts in the future.

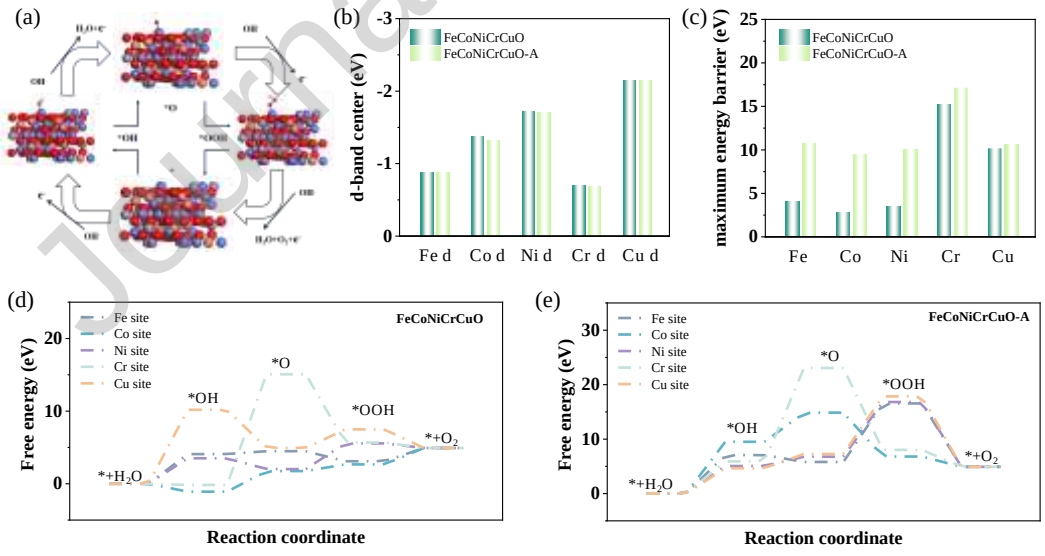

Figure 4. (a) The mechanism of OER at the surface FeCoNiCrCuO in alkaline medium (1 M KOH; Fe: purple balls, Co: blue balls, Ni: blue gray balls, Cr: grey balls, Cu: orange balls, O: red balls). (b) The calculated d-band centers. (c) The maximum energy barrier for OER of all active sites. (d, e) Free energy profile of the OER reaction path for FeCoNiCrCuO and FeCoNiCrCuO-A.

CONCLUSION

In summary, we report a high-entropy oxide FeCoNiCrCu electrocatalyst enriched with oxygen vacancies, synthesized using a non-equilibrium thermal shock stratgy. The XPS peak area associated with oxygen vacancies was substantially greater in FeCoNiCrCuO (46.9%) than in FeCoNiCrCuO-A (37.8%). Theoretical calculations indicate that the presence of oxygen vacancies can accelerate the rate determining step of OER reaction at nearby active sites, thereby reducing the overpotential of OER reaction. Consequently, the FeCoNiCrCu electrocatalyst demonstrates a relatively low OER overpotential of 256 mV at a current density of 10 $mA \cdot cm^{-2}$, accompanied by a Tafel slope measuring 48.2 $mV \cdot dec^{-1}$. Results show that a reduction in oxygen vacancy content caused by annealing deteriorates the catalytic performance, confirming the critical role of oxygen vacancies in regulating OER performance. This innovative approach to engineering high-entropy oxides provides valuable guidance for improving OER catalysts in industrial applications.

DATA AVAILABILITY

The authors declare that all the relevant data are available within the paper and its Supplementary Information file or from the corresponding author upon reasonable request.

ACKNOWLEDGEMENTS

National Natural Science Foundation of China (Grant No. 52471199).

State Key Laboratory of Precision Welding & Joining of Materials and Structures (24-

R-01).

The Postdoctoral Fellowship Program of CPSF under Grant Number GZB20240949.

AUTHOR CONTRIBUTIONS

Conceptualization, Yaotian Yan; methodology, Ruonan Liu; software, Ruonan Liu and Liang Dun; validation, Bing Qin; formal analysis, Peijia Wang; investigation, Ruonan Liu and Taili Yang; resources, Wei Cai; data curation, Ruonan Liu; writing—original draft preparation, Ruonan Liu; writing—review and editing, Shude Liu and Xiaohang Zheng; visualization, Ruonan Liu; supervision, Ruonan Liu; project administration, Shude Liu and Xiaohang Zheng; funding acquisition, Xiaohang Zheng. All authors have read and agreed to the published version of the manuscript.

COMPETING INTERESTS

The authors declare that they have no competing interests.

REFERENCE

1. He, F.; Liu, Y.; Yang, X.; Chen, Y.; Yang, C.-C.; Dong, C.-L.; He, Q.; Yang, B.; Li, Z.; Kuang, Y.; Lei, L.; Dai, L.; Hou, Y., Accelerating Oxygen Electrocatalysis Kinetics on Metal-Organic Frameworks via Bond Length Optimization. *Nano-Micro Letters* **2024,** *16* (1), 175-175.

2. Yan, Y.; Huang, K.; Lin, J.; Yang, T.; Wang, P.; Qiao, L.; Cai, W.; Zheng, X., Charge redistribution in FeOOH nanoarray by ecological oxygen-reduction deposition for boosting electrocatalytic water oxidation. *Applied Catalysis B-Environmental* **2023,** *330*.

3. Yang, S.; Liu, X.; Li, S.; Yuan, W.; Yang, L.; Wang, T.; Zheng, H.; Cao, R.; Zhang, W., The mechanism of water oxidation using transition metal-based heterogeneous electrocatalysts. *Chemical Society Reviews* **2024,** *53* (11), 5593-5625.

4. Ma, Q.; Mu, S., Acidic oxygen evolution reaction: Mechanism, catalyst classification, and enhancement strategies. *Interdisciplinary Materials* **2023,** *2* (1), 53-90.

5. Zeng, F.; Mebrahtu, C.; Liao, L.; Palkovits, R.; Beine, A. K., Stability and deactivation of OER electrocatalysts: A review. *Journal of Energy Chemistry* **2022,** *69*, 301-329.

6. Wang, H.; Zhai, T.; Wu, Y.; Zhou, T.; Zhou, B.; Shang, C.; Guo, Z., High-Valence Oxides for High Performance Oxygen Evolution Electrocatalysis. *Advanced Science* **2023,** *10* (22), e2301706-e2301706.

7. Ram, R.; Xia, L.; Benzidi, H.; Guha, A.; Golovanova, V.; Garzon Manjon, A.; Llorens Rauret, D.; Sanz Berman, P.; Dimitropoulos, M.; Mundet, B.; Pastor, E.; Celorrio, V.; Mesa, C. A.; Das, A. M.; Pinilla-Sanchez, A.; Gimenez, S.; Arbiol, J.; Lopez, N.; Garcia de Arquer, F. P., Water-hydroxide trapping in cobalt tungstate for proton exchange membrane water electrolysis. *Science* **2024,** *384* (6702), 1373-1380.

8. Zhang, X.; Wang, X.; Lv, X., Research progress of high-entropy oxides for electrocatalytic oxygen evolution reaction. *ChemSusChem* **2024**, e202401663-e202401663.

9. Gao, D.; Zhu, W.; Chen, J.; Qin, K.; Ma, M.; Shi, J.; Wang, Q.; Fan, Z.; Shao, Q.; Liao, F.; Shao, M.; Kang, Z., High-Entropy Effect Promoting Self-Healing Behavior of Two-Dimensional Metal Oxide Electrocatalysts for Oxygen Evolution Reaction. *Acs Catalysis* **2024,** *14* (5), 3700-3711.

10. Miao, K.; Jiang, W.; Chen, Z.; Luo, Y.; Xiang, D.; Wang, C.; Kang, X., Hollow-Structured and Polyhedron-Shaped High Entropy Oxide toward Highly Active and Robust Oxygen Evolution Reaction in a Full pH Range. *Advanced Materials* **2024,** *36* (8), 2308490-2308490.

11. Xiao, H.; Chi, K.; Yin, H.; Zhou, X.; Lei, P.; Liu, P.; Fang, J.; Li, X.; Yuan, S.; Zhang, Z.; Su, Y.; Guo, J.; Qian, L., Excess Activity Tuned by Distorted Tetrahedron in $CoMoO_4$ for Oxygen Evolution. *Energy & Environmental Materials* **2024,** *7* (1), e12495-e12495.

12. Wu, Y.; Guo, C.; Yao, R.; Zhang, K.; Li, J.; Liu, G., Modulating Carrier Oxygen Vacancies to Enhance Strong Oxide-Support Interaction in IrO_2/Nb_2O_{5-x} Catalysts for Promoting Acidic Oxygen Evolution Reaction. *Advanced Functional Materials* **2024**, 2410193-2410193

13. Jiang, Y.; Liang, Z.; Fu, H.; Sun, M.; Wang, S.; Huang, B.; Du, Y., Pt-Modified High Entropy Rare Earth Oxide for Efficient Hydrogen Evolution in pH-Universal Environments. *Journal of the American Chemical Society* **2024,** *146* (13), 9012-9025.

14. Wang, J.; Cheng, C.; Huang, B.; Cao, J.; Li, L.; Shao, Q.; Zhang, L.; Huang, X., Grain-Boundary-Engineered La2CuO4 Perovskite Nanobamboos for Efficient CO2 Reduction Reaction. *Nano Letters* **2021,** *21* (2), 980-987.

15. Yao, Y.; Huang, Z.; Xie, P.; Lacey, S. D.; Jacob, R. J.; Xie, H.; Chen, F.; Nie, A.; Pu, T.; Rehwoldt, M.; Yu, D.; Zachariah, M. R.; Wang, C.; Shahbazian-Yassar, R.; Li, J.; Hu, L., Carbothermal shock synthesis of high-entropy-alloy nanoparticles. *Science* **2018,** *359* (6383), 1489-1494.

16. Ye, C.; Yaling, Z.; Ziwei, Z.; Yang, L., Highly dispersed face-centered cubic copper–cobalt alloys constructed by ultrafast carbothermal shock for efficient electrocatalytic nitrate-to-ammonia conversion. *Materials Today Energy* **2022,** *29*, 101112-101112.

17. Xu, X.; Du, Y.; Wang, C.; Guo, Y.; Zou, J.; Zhou, K.; Zeng, Z.; Liu, Y.; Li, L., High-entropy alloy nanoparticles on aligned electronspun carbon nanofibers for supercapacitors. *Journal of Alloys and Compounds* **2020,** *822*, 153642-153642.

18. YeChuang, H.; MengLi, L.; Li, S.; Shuxing, L.; Gen, L.; WeiShen, S.; YanJie, W.; ZiAng, N.; SongYuan, D.; HongGang, L.; Yonggang, Y.; D, S. G.; Ru, F. F.; ZhongQun, T., A general method for rapid synthesis of refractory carbides by low-pressure carbothermal shock reduction. *Proceedings of the National Academy of Sciences of the United States of America* **2022,** *119* (37), e2121848119-e2121848119.

19. S., K. J.; Yu, M. P.; Hadas, E. M.; K., J. J.; Zhiyong, X.; Scott, H., Rapid Carbothermal Shock Enhances the Double-Layer Response of Graphene Oxide-Carbon Nanotube Electrodes. *ENERGY & FUELS* **2021,** *35* (21), 17919-17929.

20. Zheng, J.; Zhang, J.; Zhang, L.; Zhang, W.; Wang, X.; Cui, Z.; Song, H.; Liang, Z.; Du, L., Ultrafast Carbothermal Shock Constructing $Ni_3Fe_{1-x}Cr_x$ Intermetallic Integrated Electrodes for Efficient and Durable Overall Water Splitting. *ACS Applied Materials & Interfaces* **2022,** *14* (17), 19524-19533.

21. Rani, B.; Sahu, N. K., Effect of aqueous electrolytes on the supercapacitive performance of glycol-mediated $CoFe_2O_4$ nanoparticles. *Asia-Pacific Journal of Chemical Engineering* **2020,** *15* (5), e2548-e2548.

22. Yawen, H.; Gaohui, D.; Yi, F.; Lina, J.; Di, H.; Wenqi, Z.; Qingmei, S.; Bingshe, X., Prussian blue analogues-derived Ni-doped $CoFe_2O_4$ hollow nanocubes as electrocatalysts for oxygen evolution reaction. *Applied Surface Science* **2023,** *614*, 156237-156237.

23. Su, Z.; Liu, X.; Hao, S.; Li, Z.; Yang, B.; Hou, Y.; Lei, L.; Zhang, X., Pt/$CoFe_2O_4$-C hollow ball as efficient bifunctional electrocatalyst for Zn-air batteries. *Catalysis Today* **2020,** *368* (prepublish), 204-210.

24. Zuozhong, L.; Zhehao, H.; Haitao, Y.; Zhiyuan, Y.; Chaochao, Z.; Yang, X.; Wei, Z.; Haoquan, Z.; Rui, C., Quasi-single-crystalline CoO hexagrams with abundant defects for highly efficient electrocatalytic water oxidation. *Chemical science* **2018,** *9* (34), 6961-6968.

25. Bao, J.; Zhang, D. X.; Fan, B.; Zhang, J.; Zhou, D. M.; Yang, W.; Hu, X.; Wang, H.; Pan, P. B.; Xie, P. Y., Ultrathin Spinel-Structured Nanosheets Rich in Oxygen Deficiencies for Enhanced Electrocatalytic Water Oxidation. *Angewandte Chemie* **2015,** *127* (25), 7507-7512.

26. Zhao, Z.; Shao, Q.; Xue, J.; Huang, B.; Niu, Z.; Gu, H.; Huang, X.; Lang, J., Multiple structural defects in ultrathin NiFe-LDH nanosheets synergistically and remarkably boost water oxidation reaction. *Nano Research* **2021,** *15* (1), 310-316.

27. Rehman, K. u.; Airam, S.; Lin, X.; Gao, J.; Guo, Q.; Zhang, Z., In Situ Formation of Surface-Induced Oxygen Vacancies in Co_9S_8/CoO/NC as a Bifunctional Electrocatalyst for Improved Oxygen and Hydrogen Evolution Reactions. *Nanomaterials* **2021,** *11* (9).

28. Wang, Y.; Han, Y.; Suo, W.; Zhang, J.; Lai, X.; Li, Z.; Liang, Z.; Cao, G., Transition-metal oxides with peak oxygen vacancy content for oxygen electrocatalysis. *Science China Materials* **2023,** *66* (11), 4357-4366.

29. Gu, X.; Jing, H.; Mu, X.; Yang, H.; Zhou, Q.; Yan, S.; Liu, S.; Chen, C., La-triggered synthesis of oxygen vacancy-modified cobalt oxide nanosheets for highly efficient oxygen evolution in alkaline media. *Journal of Alloys and Compounds* **2020,** *814*.

30. Linzhou, Z.; Lei, G.; Yisu, Y.; Mengran, L.; Yi, J.; Xiangdong, Y.; Zhonghua, Z., Ultrathin Iron-Cobalt Oxide Nanosheets with Abundant Oxygen Vacancies for the Oxygen Evolution Reaction. *Advanced materials (Deerfield Beach, Fla.)* **2017,** *29* (17), 1606793-1606793.

31. Jahangeer, A.; Tansir, A.; Norah, A.; M.A., M. K.; Prabhakarn, A.; S., A. M.; M., A. R.; M., A. S., Reduced graphene oxide encapsulated perovskite-type lanthanum cobalt oxide nanoparticles for efficient electrolysis of water to oxygen reactions (OER/ORR). *Journal of Industrial and Engineering Chemistry* **2023,** *121*, 100-106.

32. Sharma, L.; Katiyar, N. K.; Parui, A.; Das, R.; Kumar, R.; Tiwary, C. S.; Singh, A. K.; Halder, A.; Biswas, K., Low-cost high entropy alloy (HEA) for high-efficiency oxygen evolution reaction (OER). *Nano Research* **2021,** *15* (6), 1-8.

33. Rongrong, Z.; Lun, P.; Beibei, G.; ZhenFeng, H.; Zhongxin, C.; Li, W.; Xiangwen, Z.; Zhiying, G.; Wei, X.; Ping, L. K.; JiJun, Z., Tracking the Role of Defect Types in Co_3O_4 Structural Evolution and Active Motifs during Oxygen Evolution Reaction. *Journal of the American Chemical Society* **2023,** *145* (4), 2271-2281.

34. ShuFang, L.; Jie, Z.; Liang, H.; Yao, M.; Dong, Y., Facile surface defect engineering on perovskite oxides for enhanced OER performance. *Dalton transactions (Cambridge, England : 2003)* **2023,** *52* (13), 4207–4213.

35. K., K.; Ranjith, B.; Dhanasekaran, V.; Sivalingam, R.; Soo, K. H.; Emad, A.; Akram, A.; Hyun-Seok, K., Revealing the effect of various organic ligands on the OER activity of MOF-derived 3D hierarchical cobalt oxide @ carbon nanostructures. *Journal of Alloys and Compounds* **2023,** *934*, 167909-167909.

36. Priamushko, T.; Guggenberger, P.; Mautner, A.; Lee, J.; Ryoo, R.; Kleitz, F., Enhancing OER Activity of Ni/Co Oxides via Fe/Mn Substitution within Tailored Mesoporous Frameworks. *ACS Applied Energy Materials* **2022,** *5* (11), 13385-13397.

37. Su-Ting, H.; Ye, Z.; Prashant, S.; Huaixin, W.; Li, Z.; Yan, Y.; Chun-Sing, L.; L, R. V. A., Surface engineering of reduced graphene oxide for controllable ambipolar flash memories. *ACS applied materials & interfaces* **2015,** *7* (3), 1699-708.

38. Chengyan, Z.; Xu, H.; Fengyuan, Z.; Xiaoli, Z.; Yidong, L.; Jiangping, L.; Xueqin, C.; Hongwei, G., Facile synthesis of the encapsulation of Co-based multimetallic alloys/oxide nanoparticles nirtogen-doped carbon nanotubes as electrocatalysts for the HER/OER. *International Journal of Hydrogen Energy* **2022,** *47* (65), 27775-27786.

39. Khan, G. Z.; Khaled, E.; Mohamed, M. N.; Ahmed, B.; Yiming, W.; Ahmed, A.-W., Incorporation of manganese carbonyl sulfide ($(Mn_2S_2(CO)_7)$) and mixed metal oxides-decorated reduced graphene oxide ($MnFeCoO_4$/rGO) as a selective anode toward efficient OER from seawater splitting under neutral pH conditions. *Renewable Energy* **2022,** *190*, 1029-1040.

40. Yang, Z.; Xiang, X.; Yang, J.; Zhao, Z.-Y., High-entropy oxides as energy materials: from complexity to rational design. *Materials Futures* **2024,** *3* (4).

41. Chen, H.; Wu, W.; Chen, S.; Wang, Z.; Chen, R.; Cheng, N., Tailoring the d-band center of porous CoS_2 nanospheres via low-electronegative Fe for weakened OH* adsorption and boosted oxygen evolution. *Inorganic Chemistry Frontiers* **2023,** *10* (19), 5668-5677.

42. Yang, J.; Yang, S.; An, L.; Zhu, J.; Xiao, J.; Zhao, X.; Wang, D., Strain-Engineered Ru-NiCr LDH Nanosheets Boosting Alkaline Hydrogen Evolution Reaction. *ACS Catalysis* **2024,** *14* (5), 3466-3474.

43. Salem, K. E.; Saleh, A. A.; Khedr, G. E.; Shaheen, B. S.; Allam, N. K., Unveiling the Optimal Interfacial Synergy of Plasma-Modulated Trimetallic Mn-Ni-Co Phosphides: Tailoring Deposition Ratio for Complementary Water Splitting. *Energy & Environmental Materials* **2022,** *6* (2), e12324-e12324.

44. Streibel, V.; Schönecker, J. L.; Wagner, L. I.; Sirotti, E.; Munnik, F.; Kuhl, M.; Jiang, C.-M.; Eichhorn, J.; Santra, S.; Sharp, I. D., Zirconium Oxynitride Thin Films for Photoelectrochemical Water Splitting. *ACS Applied Energy Materials* **2024,** *7* (9), 4004-4015.

45. Yu, G.; Yuzhi, L.; Haiyang, Y.; Donglei, Z., High-entropy oxides for catalysis: status and perspectives. *Applied Catalysis A: General* **2022,** (prepublish), 118478-118478.

Declaration of Interest Statement

The authors declare that they have no competing interests.